Proceedings of ASME Turbo Expo 2019: Turbomachinery Technical Conference and Exposition
GT2019
June 17-21, 2019, Phoenix, Arizona, USA

GT2019-91245

PARAMETRIC STUDY ON PORTED SHROUD LOCATIONS AND GEOMETRIES FOR A TURBOCHARGER COMPRESSOR

Suheab Thamizullah[#]
IIAEM, Jain University
Bengaluru, KA, India

Abdul Nassar
SoftInWay Turbomachinery Solutions Pvt. Ltd.
Bengaluru, KA, India

Antonio Davis
IIAEM, Jain University
Bengaluru, KA, India

Gaurav Giri
SoftInWay Turbomachinery Solutions Pvt. Ltd.
Bengaluru, KA, India

Leonid Moroz
SoftInWay Inc.
1500 District Ave, Burlington MA, 01803, USA

ABSTRACT

Turbochargers are commonly used in automotive engines to increase the internal combustion engine performance during off-design operating conditions. When used, the widest operating range for the turbocharger is desired, which is limited on the compressor side by the choke condition and the surge phenomenon. The ported shroud technology is used to extend the operable working range of the compressor, by permitting flow disturbances that block the blade passage to escape and stream back through the shroud cavity to the compressor inlet. The impact of this technology, on a speed-line, at near optimal operating condition, near choke operating condition and near surge operating condition is investigated.

The ported shroud (PS) self-recirculating casing treatment is widely used to delay the onset of surge by enhancing the aerodynamic stability of the turbocharger compressor. While the ported shroud design delays surge, it usually comes with a small penalty in efficiency.

This research involves designing a single-stage centrifugal compressor for the given specifications, considering the application of an automotive turbocharger. The ported shroud was then introduced in the centrifugal compressor. The performance characteristics were obtained, both at the design and at off-design conditions, both with and without the ported shroud. The performance was compared at various off-design operating speed lines. The entire study, from designing the compressor to optimizing the ported shroud configuration, was performed using the commercial AxSTREAM® software platform. Parametric studies were performed to study the effect of ported shroud axial location along the blade axial length on the operating range and performance. The baseline design, without the ported shroud (P0), and the final geometry with it for all PS inlet axial locations (P1 to P5) were analysed using a commercial CFD package and the results were compared with those from the streamline solver.

NOMENCLATURE

Ae	Impeller exit area
C_{in}	Ported Shroud inlet axial length from impeller inlet
CP	Choke Point on a specific Speed line
Di	Compressor inlet diameter
De	Exducer diameter
D1h	Inlet wheel diameter at hub
D1t	Inlet wheel diameter at tip
D2h	Outlet wheel diameter at hub
DoE	Design of Experiments
IC	Internal Combustion
L	Impeller axial length
PD	Preliminary Design
PS_{in_loc}	Ported Shroud slot inlet location
PS	Ported Shroud
Qin	Inlet volume flow
Tout,0	Total temperature at the outlet boundary
Utip	Blade tip speed

INTRODUCTION

With increase in urban traffic and increased idling or lower speed operation of the engine during slow traffic, engine manufacturers are demanding higher operating range for the turbochargers with better performance at lower mass flow conditions. This has forced turbocharger designers to explore possible ways of increasing the operating range and efficiency especially at deep off-design operation. The range of a turbocharger is limited by the compressor choke and surge characteristics. The inclusion of ported shroud helps in extending this operating range.

A ported shroud (PS) is similar to a self-recirculating casing treatment that consists of a cavity in the inducer shroud with its inlet downstream of the inducer throat and its outlet upstream of the impeller leading edge. A fraction of the flow in the impeller enters the cavity and recirculates either to the upstream of the impeller or bypasses a fraction of the flow from the inlet to impeller depending on the pressure differential as shown in Figure 1. The placement of the end locations of the cavity are selected in such a way as to provide a positive

[#]Current affiliation: SoftInWay Turbomachinery Solutions Pvt. Ltd.

pressure differential between the outlet and inlet of the PS cavity near choke and a negative pressure differential near stall operation. The presence of positive pressure differential allows some of the inlet flow to bypass the inducer throat (Figure 1A) at choke flow. During stall/surge, a fraction of the flow recirculates through the cavity to the inlet due to higher static pressure (Figure 1B) thus preventing a separation of flow at the inlet by maintaining a higher flow through the compressor inlet than required at the outlet of the compressor.

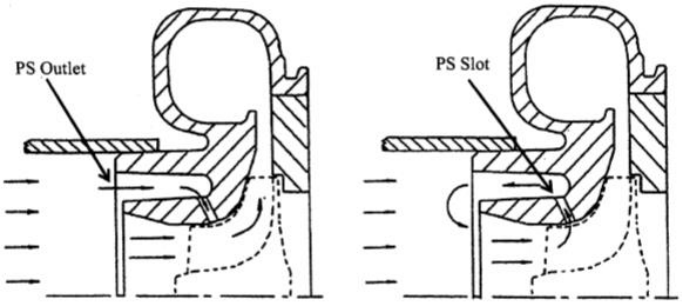

(A) Near choke **(B) Near Surge**

Figure 1: Schematic of the ported shroud operation [1]

Few studies have been reported on the flow physics of the ported shroud at near surge operation of the compressor stage using computational methods. Chen and Lei [2] reviews the development of the ported shroud concept from its first conception in the 1980s to its various configurations currently available along with the details of the underlining mechanisms that deliver the performance improvement. Ramachandran et.al., [3] reports on the performance improvement of a compressor stage at low flow region. The improvement was achieved through a set of designed experiments using a combination of preliminary design and CFD tools. Efficiency improvement of about 7% was observed in the lower flow range while there was a drop of about 3.7% near the peak power operating point. The performance evaluation, at different speed lines, showed that the modified compressor had higher part load efficiencies. Sharma et. al., [4] presents an investigation of the flow processes associated with a ported shroud compressor and quantifies the effect of these flow mechanisms on the compressor operation. Numerical simulation of a full compressor stage, using multiple reference frames, was performed using a Reynolds Averaged Navier-Stokes (RANS) solver with shear stress transport (SST) turbulence model for steady state conditions at the design and near surge operation. Semlitsch et. al., [5] performed numerical analysis of the flow-field, with and without the ported shroud, in a centrifugal compressor at near optimal efficiency and near-surge operating conditions using Large Eddy Simulation (LES). Flow separation and recirculation bubbles were accurately predicted by the LES approach. It shows that LES predicts the flow structure better than (RANS) simulation.

Guillou et. al., [6] reports on the relationship between inlet flow recirculation and instability control using stereoscopic particle image velocimetry (PIV) in conjunction with dynamic pressure transducers at the inlet of the turbocharger compressor with and without the ported shroud. Both stable and unstable operating points were analysed using phase-locked PIV measurements during surge. Rather than one-dimensional, the surge flow is characterized by a three-dimensional structure of both entering and exiting swirling flows, alternating in magnitude during a self-excited pressure cycle. The correlation between pressure and velocity measurements shows that the development of compressor unsteadiness is concurrent with swirling reversed flow at the impeller tip. The impact of the ported shroud on the inlet velocity flow-field is evident by the presence of localized flow recirculation. Christou et. al., [7] performed studies on a centrifugal compressor, with and without the ported shroud of different geometrical configurations, to establish a link between the flow effects in the ported shroud cavity and compressor performance changes. It was shown that the main flow path perceives the ported shroud flow as a combination of flow actuations, including injection and removal of mass flow, and injection of axial as well as tangential momentum, thus altering the main flow.

In the present work, a turbocharger compressor stage was designed based on the technical specifications (Table 1) of a passenger car engine using the AxSTREAM® software (design tool). Subsequently, a ported shroud was introduced to compare the performance, at design and off-design operations, with and without the ported shroud. Parametric study, on the location of the ported shroud, was performed using both 1D and 3D tools to establish the optimal location in terms of the performance, considering operating condition at near surge and at choke. The operating envelope is determined based on the boost pressure and mass flow rate required by the IC engine during various operating conditions as specified by the engine manufacturer.

Table 1: Technical specification compressor design

Parameter	Value	Unit
Inlet total temperature	296	K
Inlet total pressure	101.3	kPa
Static pressure at outlet	156	kPa
Mass flow rate	0.27	$kg.s^{-1}$
Shaft rotational speed	64000	rpm
Rotor outlet tip diameter	<84	mm
Rotor hub diameter	>20	mm

COMPRESSOR DESIGN AND OPTIMIZATION

The compressor stage was designed from clean sheet using the commercial turbomachinery design platform that encompasses the complete process of turbomachinery flow path design starting from initial stage sizing to 3D geometry generation [8]. The flow chart presented in Figure 2 depicts the design process that starts from the preliminary design module, where the inputs are boundary conditions, geometric parameters, design parameters and constraints [9]. The geometric and design parameters are specified in a range that allows generating multiple designs using a random sequence search method based on an inverse task solver. The output from the preliminary design module is initial flow path of the

compressor stage along with the performance parameters, such as kinematic and thermodynamic results and losses as well as the overall performance in terms of mass flow, pressure ratio and efficiency at various speed lines. The obtained feasible flow path is then analysed in the detailed design process using meanline/streamline and full streamline analysis. The off-design performance is also calculated during this phase, for different speed lines, to establish the operating range. Design of Experiment (DoE) based optimization can also be performed during this step and, subsequently, 3D blade design is completed by profiling the individual blade sections. A quick CFD analysis for each of the profiled section is performed using CASCADE CFD before full 3D CFD analysis is performed. This results in shorter design cycle time.

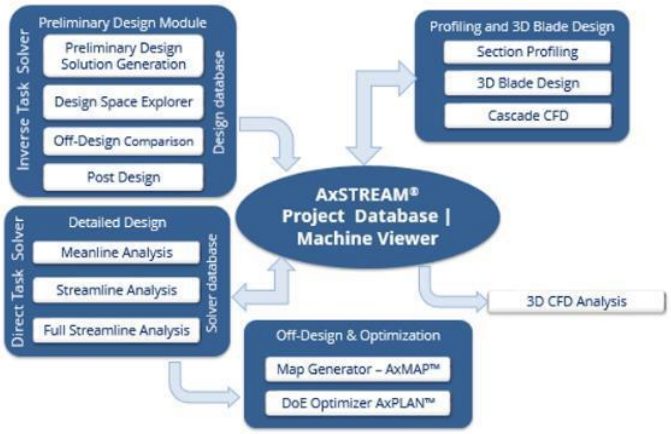

Figure 2: The process flow chart for designing centrifugal compressor in AxSTREAM® platform [8]

Table 2: Range of geometrical parameters for design

Parameter	Units	Value
Inlet mean diameter	mm	40– 60
Rotor diameter ratio	-	1.5– 2.2
Flow factor	-	0.3– 0.8
Meridional velocity gradient	-	0.8– 1.2
Rotor blade exit angle	deg.	50 - 70

Table 3: Loss model settings

Parameter	Loss model used
Primary loss (Profile)	Aungier Loss model
Deviation angle calculation	Weisner loss model
Blockage calculation	AxS default (SoftInWay)
Tip leakage calculation	AxS default (SoftInWay)

In addition to the specifications listed in Table 1, additional inputs for the preliminary design are presented in Table 2. The inverse task solver in PD is based on 1-dimensional calculation and the accuracy of results depends on the loss model selection. Based on the recommendations in user documentation [8], the loss models listed in Table 3 were selected for the present design and analysis. Hundreds of designs were generated to evaluate the performance and geometry influencing parameters. Subsequently, constraints were applied to choose the most optimal solutions from the design space. All initial designs were performed without considering ported shroud.

Figure 3 shows the generated designs presented as a function of flow coefficient and work coefficient, colour contoured by the total-to-total efficiency. It is observed that the designs with lower flow coefficient and higher work coefficient have better efficiency for these boundary conditions and geometric parameters.

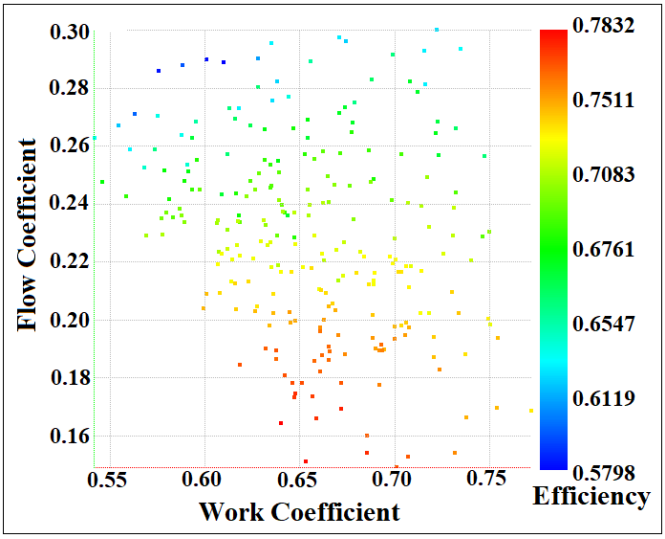

Figure 3: Design space for the different solutions generated plotted as function of flow coefficient and work coefficient

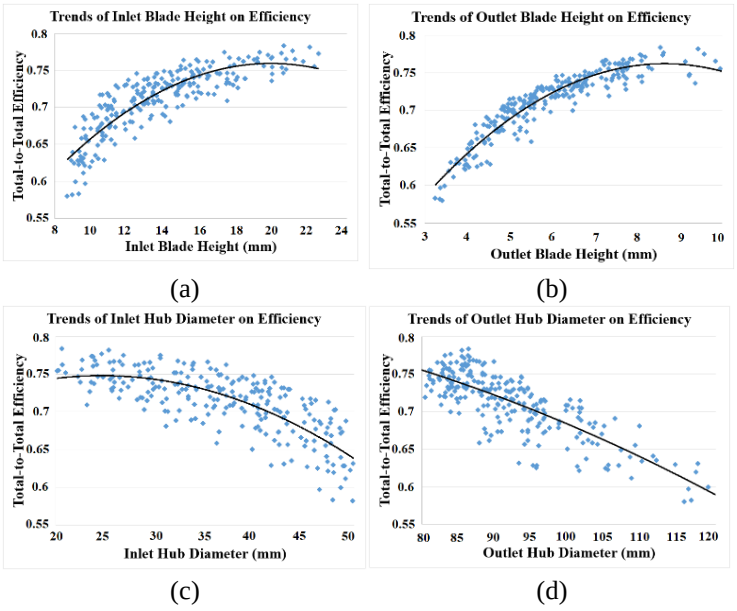

Figure 4: Effect of geometric parameters on efficiency for the different generated designs

The various influencing geometric parameters are presented in Figure 4. From (Figure 4a), it is observed that an increases in inlet blade height of the impeller results in the rise of efficiency with an optimal value of inlet blade height lying

between 20 to 24 mm. Similarly, the outlet blade heights between 8 to 10 mm give the highest efficiency (Figure 4b). The lower the inlet hub diameter, the better the performance (Figure 4c) and the same stands true for the outlet hub diameter as well (Figure 4d). Based on the desired performance in terms of pressure ratio and mass flow, additional geometric constraints were imposed to filter out the designs that do not meet the desired performance at both design and off-design conditions. One design was chosen, from the various generated designs, for detailed design and optimization. Table 4 lists the geometric parameters for the selected design.

Table 4: Geometric parameters of the initially selected impeller

Parameter	Unit	Value
Inlet hub diameter	mm	23.61
Inlet tip diameter	mm	64.42
Outlet diameter	mm	84.63
Inlet channel height	mm	20.40
Outlet channel height	mm	8.71
Inlet angle at hub, mean and tip	deg.	46.26|29.28|20.96
Outlet angle at hub, mean and tip	deg.	52.06

The detailed design was performed using the 1D/2D streamline calculation module which is based on axisymmetric analysis. It offers different problem formulations and solver options (meanline and full streamline analysis) [8]. The flow path geometry was fine-tuned further by minor adjustments in the flow path dimensions. A DoE based optimization, using the Box and Behnken mathematical model, was then performed for the parameters as listed in Table 5 with efficiency, mass flow rate and pressure ratio as the objectives of the optimization to ensure the design targets and requirements were met. Here, the inlet and outlet metal angles are relative to the tangential direction. The DoE generated a response surface from which the optimal solution was selected for further studies.

Table 5: Design of experiments variables

Parameters for optimization	Unit	Range	Optimal value
Inlet tip diameter of impeller	mm	65 – 72	71.94
Impeller outlet metal angle	deg.	46 – 57	52.84
Impeller inlet metal angle	deg.	26 – 32	28.64
Number of blades	-	6 – 9	8
Impeller axial length	mm	25 – 30	29
Impeller blade exit height	mm	7 – 10	8.98

The performance map of the designed compressor, for different speed lines, generated using the meanline analysis, is presented in Figure 5. Figure 5(b) shows the performance in terms of pressure ratio and mass flow for 3 speed lines of 58,000 rpm, 64,000 rpm and 70,000 rpm. Figure 5(a) shows the efficiency at the same three speed lines plotted against the mass flow rate.

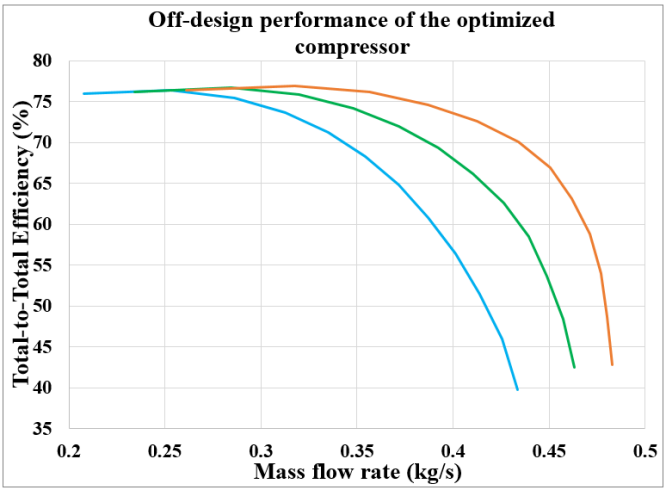

(a) Efficiency versus mass flow rate

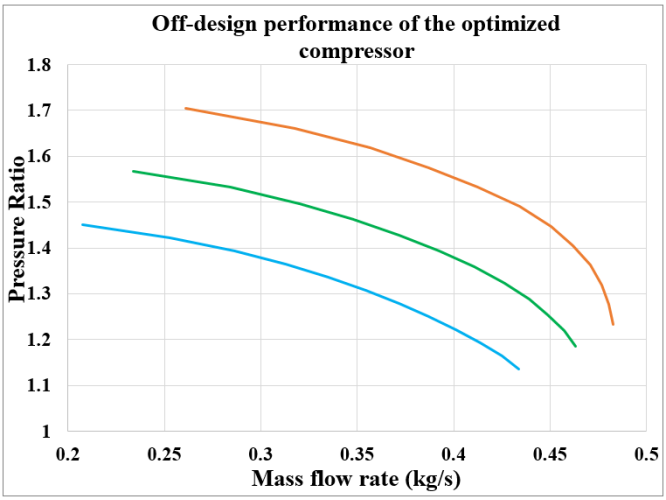

(b) Pressure ratio versus mass flow rate

Figure 5: Performance map of the optimized baseline compressor

PORTED SHROUD DESIGN

To increase the operating margin towards surge, ported shroud was introduced to the baseline compressor. The ported shroud was included first for 1D analysis by activating the option to include recirculation and specifying the required geometric information of the ported shroud. The initial location of the cavity inlet was specified as 4.55 mm from the inlet of the impeller in the axial direction. The equivalent cavity area was specified as 500 mm^2 which was calculated based on equation 1.

$$A = \pi D_t b_{bs} \quad (1)$$

where, A is the equivalent cavity area, D_t is the tip diameter of the impeller at inlet of the slot, b_{bs} is the width of the slot inlet.

Based on these inputs, the required model was generated for analysis of the ported shroud. The geometry of the compressor flow path, along with ported shroud representation, is shown in Figure 6.

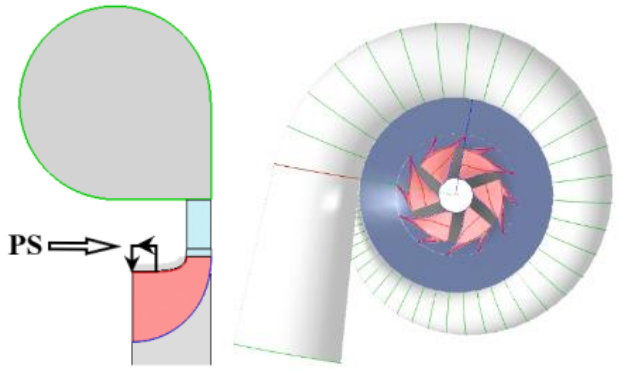

Figure 6: Compressor flow path diagram with ported shroud

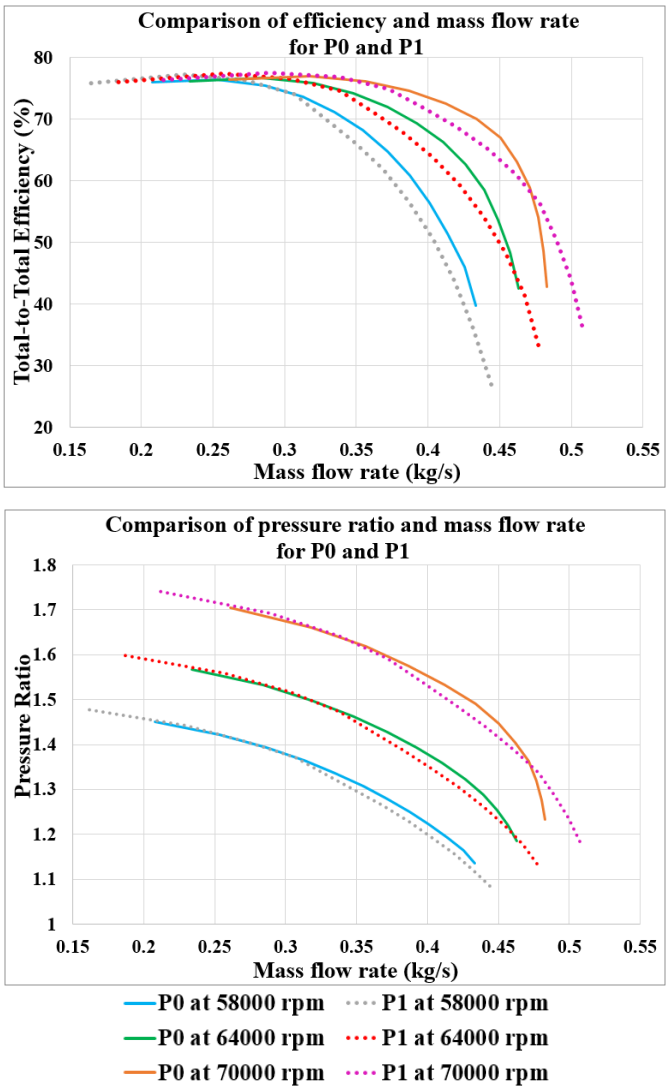

Figure 7: Performance comparison of ported shroud compressor with baseline compressor for different speed lines

Figure 7 shows the performance comparison of the compressor with ported shroud (designated as P1) with the baseline compressor (designated as P0) for three different speed lines. The axial location of the ported shroud compared here is 4.5 mm from impeller inlet. From Figure 7, it is evident that the introduction of ported shroud for the baseline compressor has increased the surge and choke margin at all operating speeds. At 58000 rpm, the surge margin and choke margin have increased by 17.64% and 3.83% respectively, compared to the baseline compressor. At the design speed of 64000 rpm, the surge and choke margins have increased by 20.01% and 5.18% respectively. At 70,000 rpm, the surge and choke margins have increased by 18.93% and 9.16% respectively. At the same time, there is 5.15% drop in efficiency for 58000 rpm, while for 64000 rpm and 70000 rpm there is an improvement in efficiency of 1.03% and 11% respectively at choke condition for the same mass flow rate, compared to the baseline case. The percent difference between the two configurations (P0 and P1) for the same mass flow rate at all three speeds is listed in Table 6. The surge and choke margin was calculated based on equations (2) and (3).

$$\text{Surge Margin} = \frac{\dot{m}_o - \dot{m}_s}{\dot{m}_o} \quad \textbf{(2)}$$

$$\text{Choke Margin} = \frac{\dot{m}_c - \dot{m}_o}{\dot{m}_o} \quad \textbf{(3)}$$

where, $\dot{m}_o$ is the design mass flow rate, $\dot{m}_s$ is the surge mass flow rate and $\dot{m}_c$ is the choke mass flow rate.

Table 6: Comparison of compressor performance (in percentage) with and without ported shroud at different speeds

RPM	Difference between P0 and P1			
	Surge Margin (%)	Choke Margin (%)	Surge Efficiency (%)	Choke Efficiency (%)
58000	+17.64	+3.83	+0.79	**-5.15**
64000	+20.01	+5.18	+0.73	+1.03
70000	+18.93	+9.16	+0.66	+11.00

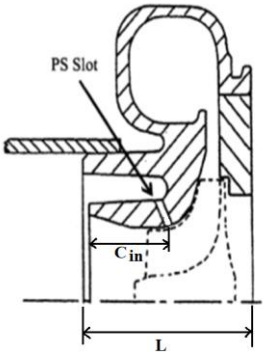

$PS_{in\_loc} = C_{in} / L$

P1 = 0.15

P2 = 0.30

P3 = 0.40

P4 = 0.50

P5 = 0.60

Figure 8: Location of axial position of ported shroud

Further to this, to identify the influence of the ported shroud inlet location, parametric study on shroud cavity inlet axial location was performed. Five different axial locations were

considered for the present analysis. The configurations designated based on shroud cavity inlet locations are presented in Figure 8. The ported shroud location (PS_{in_loc}) is calculated as relative position of the ported shroud inlet axial location (C_{in}) from the impeller inlet to the total axial length of the impeller (L).

$$PS_{in\_loc} = C_{in} / L \quad \textbf{(4)}$$

The geometry without ported shroud is designated as P0. The locations used are 0.15, 0.3, 0.4, 0.5 and 0.6 which are designated as P1, P2, P3, P4 and P5 respectively. The results from meanline calculation, for all the configurations, are presented in Figure 9 for the design speed. From Figure 9, it is evident that the surge and choke margins have increased with the introduction of ported shrouds. There is also a small decrement in efficiency, especially at off-design conditions. Optimum surge margin and choke margin are found for case P1. Table 7 lists the comparison of the different configurations against baseline compressor performance in terms of percentage change in surge and choke margin, and efficiency at same mass flow conditions.

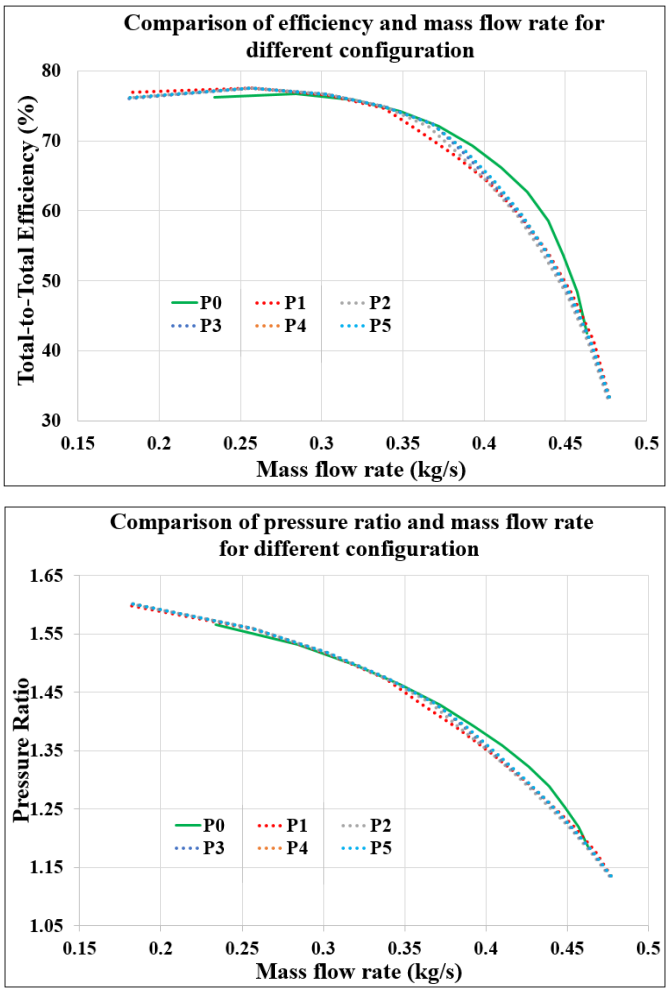

Figure 9: Performance comparison of baseline compressor with different ported shroud configuration

Table 7: Performance of ported shroud at various location

Location	Percentage difference against baseline			
	Surge margin (%)	Choke margin (%)	Efficiency (%)	
			Surge	Choke
P0	0	0	0	0
P1	+20.01	+5.18	+0.73	+1.03
P2	+19.10	+4.72	+0.84	**-0.89**
P3	+19.75	+5	+0.88	**-0.25**
P4	+19.54	+5.04	+0.89	+0.09
P5	+19.51	+5.05	+0.90	+0.15

CFD ANALYSIS

To analyse the designed compressor and to verify the performance, 3D CFD analysis was performed for all configurations including the baseline case. CFD analysis provides an insight into the flow behaviour within the compressor passage and an in depth understanding on the physics of the flow. The results of the CFD calculations were compared with meanline analysis. To reduce computational resources and time, CFD modelling of the flow domain was done considering only the impeller and vane-less diffuser. The volute geometry was excluded from all configurations for which CFD analysis was performed. The ported shroud geometry for CFD analysis was modelled in CAD package.

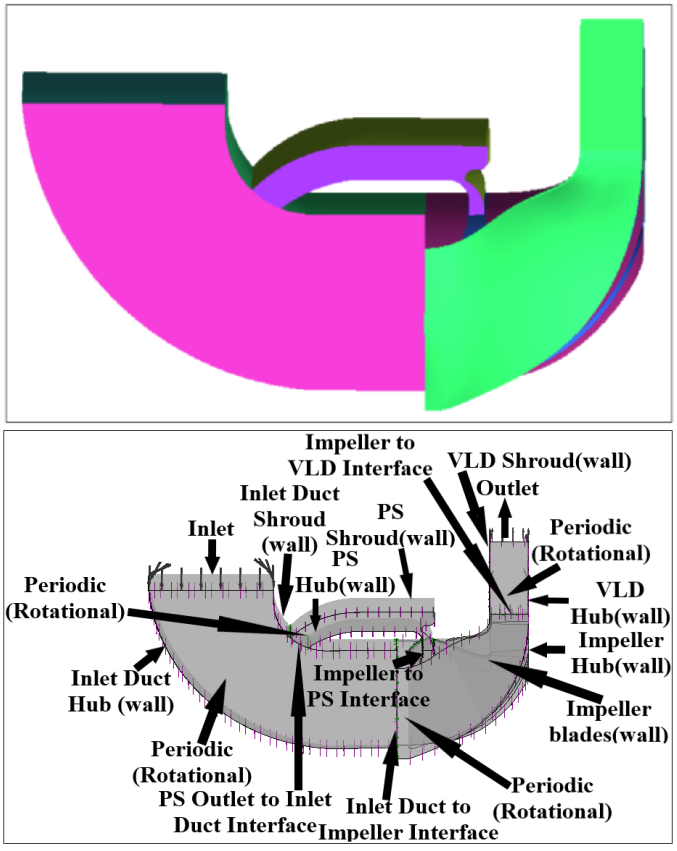

Figure 10: Flow path model of the compressor with ported shroud and boundary conditions for CFD analysis

The fluid domain was extracted and meshed and CFD analysis was performed using commercial CFD code. In each geometry with ported shroud, an additional intake duct was modelled so that the flow from the ported shroud cavity had a sufficient region at the intake to stabilize. It also ensures that no numerical instability was included in the analysis due to shorted inlet region. Grid convergence study has been carried out using 4 different number of total mesh elements and it was decided to use case with the number of elements as 934008 elements for further studies. The y+ value for area of interest (blades, walls and cavity) is less than 4 and throughout the domain its value is less than 10. The turbulence model used is k-ω for all the cases. The flow domain for the model with ported shroud (case P1) is shown in Figure 10. It is a mixed geometry with rotating and stationary domains, only impeller zone is rotating domain and other domains such as vane less diffuser, ported shroud cavity and intake duct are stationary domains. The boundary characteristics assigned for the CFD analysis are also presented in Figure 10.

The performance comparison of the results from CFD with meanline solver, for all cases and for the design speed, is presented in Figure 11. Since the volute has not been included in 3D CFD calculation, the comparison presented in Figure 11 and Table 8, with the meanline solver is also without the volute. It is evident, from both CFD and meanline analysis results, that the introduction of ported shroud for baseline compressor has increased the surge and choke margin but with negligible change in efficiency at off-design conditions. The percentage difference between meanline and CFD results are listed in Table 8 for all configurations.

Table 8: Comparison of meanline and CFD results

Configuration	Pressure ratio (%)			Efficiency (%)		
	Surge	Design	Choke	Surge	Design	Choke
P0	+4.42	+3.22	+13.43	+3.43	+0.80	**-13.84**
P1	+3.33	+3.31	+25.12	+6.42	+1.25	+4.97
P2	+4.47	+3.75	+28.04	+8.20	+1.16	+1.23
P3	+4.93	+4.42	+27.60	+8.22	+2.80	+0.62
P4	+5.46	+5.32	+30.20	+9.68	+4.25	+1.95
P5	+7.16	+7.27	+31.94	+11.29	+6.00	**-0.22**

CFD predictions are taken as the reference for the difference comparison. It is observed that the pressure ratio between CFD and meanline solver for various configurations from design to stall/surge has a variation of 3 to 7% with meanline solver predicting higher than the CFD calculation. At the same time, near choke condition the variation is higher than 7%. The efficiency comparison at design condition for different configuration shows a difference of 0.8 to 6 percent between the meanline solver and CFD results with meanline solver predicting higher efficiency. Whereas at the surge condition the efficiency varies comparison between meanline and 3D CFD shows a variation of about 3.4 to 11.3 % for different configurations. Again at the choke condition, the difference in efficiency between meanline solver and 3D CFD varies from almost 0 to 4% for the ported shroud configuration and for baseline the efficiency in the meanline solver is under-predicted by 13.8%. It is to be observed that as the axial distance of the ported shroud inlet (referenced from the impeller inlet) increases the difference in prediction between meanline solver and 3D CFD. It is also to be noted that the losses in the cavity for various configurations used has been kept constant in the meanline solver, however from the CFD results it is observed that with the change in ported shroud location the losses in the ported shroud cavity increases and this factor needs to be accounted for in the meanline solver. Ramachandran [3] has performed experimental and CFD analysis of the ported shroud compressor stage with volute using the same meanline solver and has reported good agreement between meanline solver and test results.

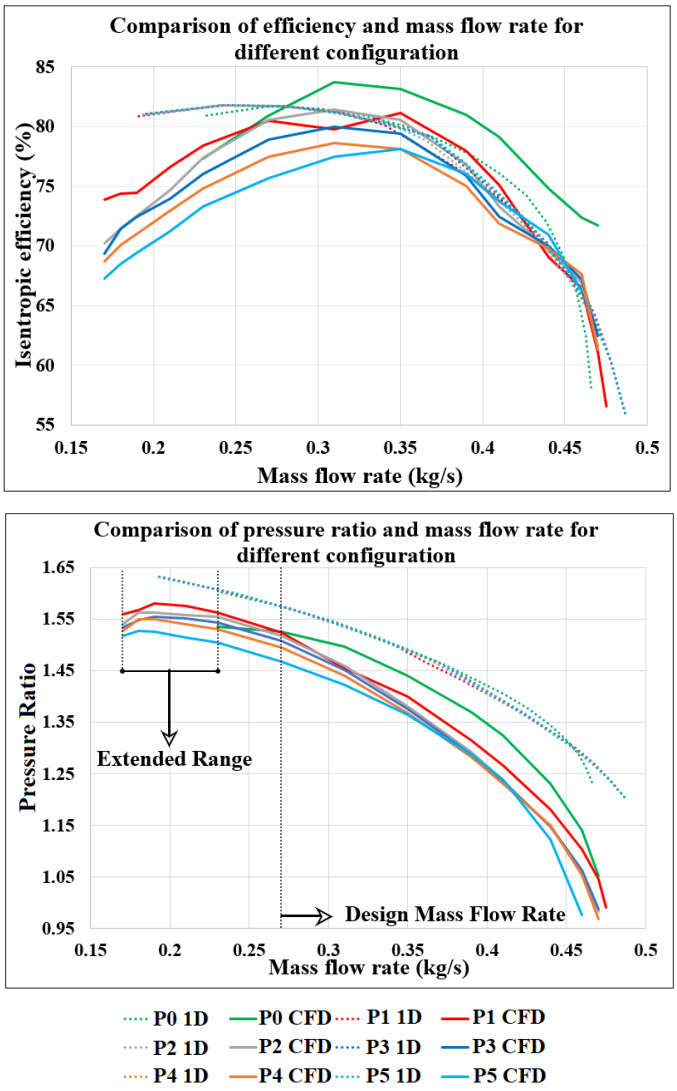

Figure 11: Comparison of meanline and CFD results for different cases of ported shroud and baseline compressor

From the results of CFD and meanline solver it can be concluded that to achieve a better performance with ported shroud, the cavity location should be selected closer to inducer

outlet and as close as possible to the impeller inlet section and should not extend into the impeller region.

CFD RESULT FURTHER ANALYSIS

For in-depth post-processing and for understanding of the flow features within the compressor flow path, meridional planes were created as shown in Figure 12. The planes 1, 2 and 3 for case with ported shroud and are located at 30%, 60% and 90% from the inlet of the intake duct, respectively. For the baseline case without ported shroud there is no intake duct so planes 1 to 3 were excluded in the baseline case. Planes 4, 5, 6, 7, 8 and 9 are located in the rotor (inducer + impeller) at 1%, 20%, 40%, 60%, 80% and 99% respectively from inducer inlet for all the configurations. Planes 10 and 11 in the vane-less diffuser and are located at 50% and 99% from the vane-less diffuser inlet.

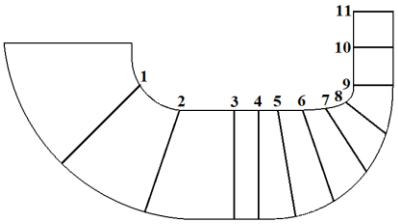

Figure 12: Plane locations for post processing of CFD results

The contours of relative Mach number in rotating frame are presented for configurations with and without ported shroud near surge, at design point and near choke from Figures 13 through Figure 16. Figure 13 shows the contours of relative Mach number at the design point without ported shroud (a) and with ported shroud (b). Since the flow at the inlet duct without ported shroud is uniform at, the planes 1, 2 and 3 are plotted only for configurations with ported shroud. The flow in case of compressor without ported shroud (Figure 13a) is uniform until it approaches the blades leading edge (plane 4). As the flow migrates from plane 4 to plane 5, separation of the flow near the tip region can be observed due to interaction of tip leakage flows with the end wall boundary layers along the meridional direction. This separated flow forms into a vortex of low momentum fluid which is carried further along the flow as it approaches the splitter blade as can be seen in plane 7. The vortex traverses from the tip towards the hub region and exits the blade passage as observed in the subsequent planes as the flow direction through the blade changes into radial direction and enters the vane-less diffuser. In Figure 13b, at design point the flow upstream of the impeller in the intake duct is uniform. However, as it approaches the leading edge of the blade, the flow structure is significantly different from the case without the presence of the ported shroud. The flow which is sucked downstream of the inducer is injected upstream of the inlet thus significantly reducing the low momentum fluid that is formed near the tip region in case of a compressor without ported shroud. As the flow travels meridional through the blade passage, it is observed that the flow vortex with low momentum fluid which is present in the case without ported shroud near the tip region is not present in the case with ported shroud. As the flow travels further (plane 6), there is no major change in flow structure except for the increase in relative Mach number due to energy addition in impeller and change in area. On planes 7, 8 and 9, as relative Mach number increases and flow turning happens, there is flow separation due to curvature and boundary layer formation along the main and splitter blades.

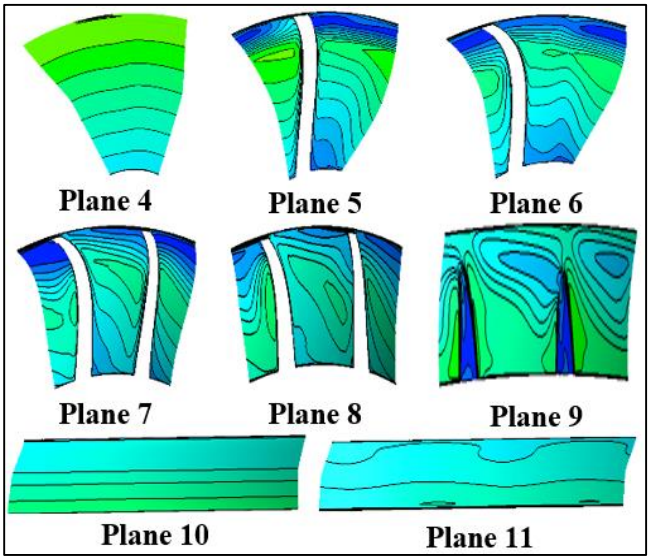

(a) without ported shroud

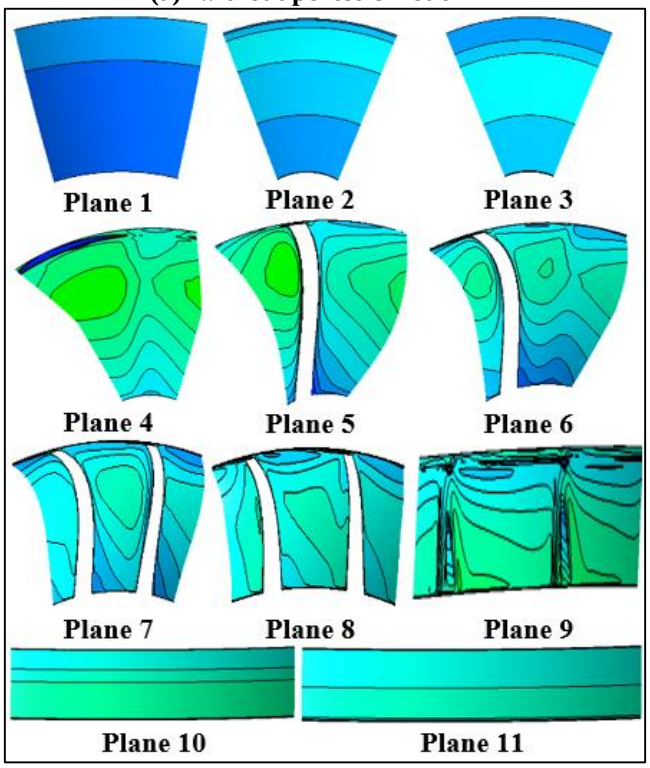

(b) with ported shroud

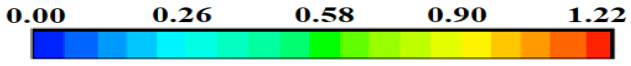

Figure 13: Relative Mach number contours for with and without ported shroud for design condition

As the flow travels further towards the exit, it tends to get uniform without any major vortex regions as seen through planes 10 and 11. Due to the reduced separation of the flow near the tip, the ported shroud geometry is able to produce higher surge margin with slightly higher efficiency.

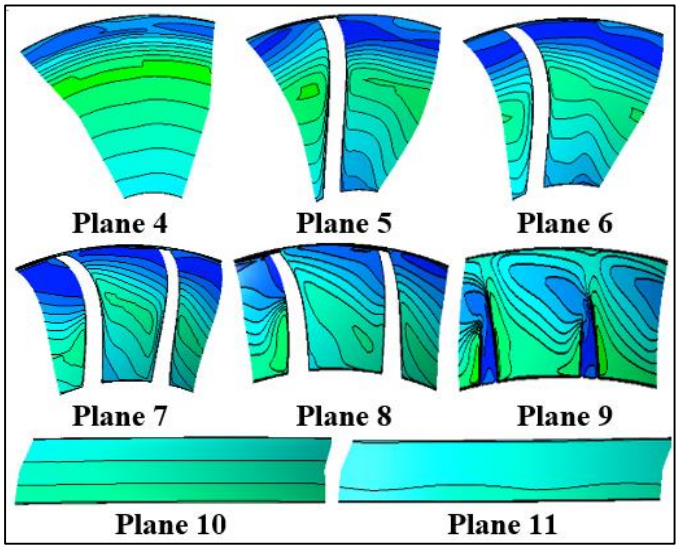

(a) without ported shroud

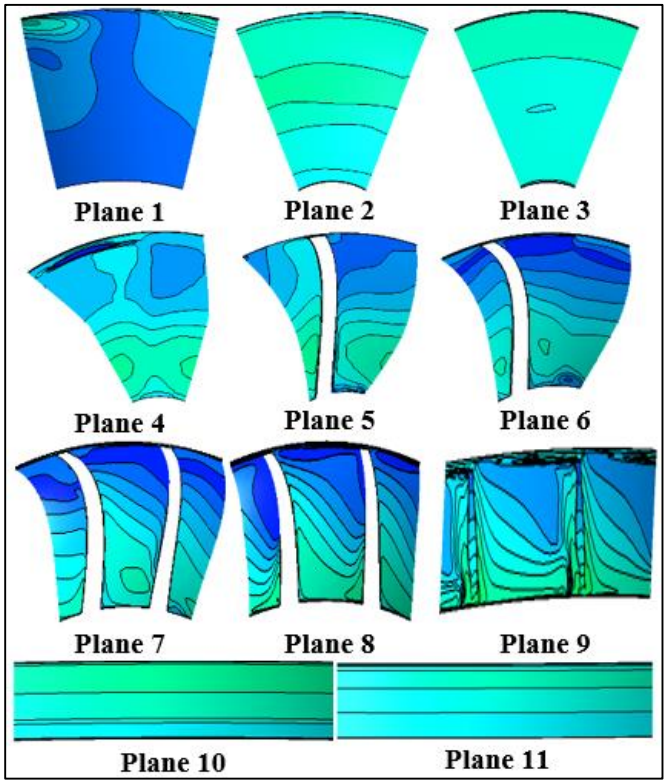

(b) with ported shroud

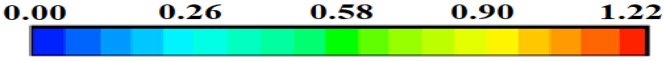

Figure 14: Relative Mach number contours for with and without ported shroud for near surge condition

Figure 14 shows the contours of relative Mach number near surge for compressor without ported shroud (a) and with ported shroud (b). The flow at the plane 1 for the case with ported shroud is distorted due to the mixing of the main flow with the high pressure fluid that is being injected into the intake through the ported shroud cavity. The distortion that is observed in plane 1 gets smoothened as it flows through the intake duct towards the leading edge of the impeller. In the case without ported shroud, the flow as it enters the impeller has a larger region of separated flow towards the tip region due to the lower mass flow condition near surge compared to the design condition (Figure 13). Due to presence of large separated flow near surge condition within the impeller passage, the efficiency is lower for the surge condition.

Figure 14b shows the relative Mach number contours with ported shroud configuration for near surge condition. The flow at the inlet duct shows a mixing of the main flow and flow exiting through the cavity of the ported shroud. This mixing causes a disturbance which can be observed in plane 1. Though there exists a flow separation in the blade passage on the suction side, the structure of the vortex that exists in the case with ported shroud is smaller. This results in better flow quality compared to the case without ported shroud. It can be said that the extraction of the fluid near the tip region, through a ported shroud, results in improved flow structure through the blade passage. The separation of the flow on the suction surface still exists like in the case without the ported shroud, but now there is a migration for the region of separated flow inside the impeller passage with the hub section having the larger chunk of the low momentum fluid. The interaction of the leakage flow, the suction created by the ported shroud and the vortices formed at the tip region result in slight reduction in the flow velocity at the tip region.

Figure 15 presents the meridional velocity in the blade passage which is normalized along the blade to blade and hub to tip plane to give a more clear understanding on how the flow progresses through the impeller passage without ported shroud (a) and with ported shroud (b). The velocity of the flow, before it approaches the blade, is more uniform with a low velocity region near the tip due to the boundary layer at the shroud. The velocity at the suction side is higher than that at the pressure side from hub until it approaches about 60% of the span. Above that, there is a reduction in velocity due to the separated flow near the tip as observed in Figure 14a. The suction side velocity for both splitter and main blades reduces towards the tip on plane 7 due to the wake formed by the mixing of the boundary layer flow and the tip clearance flow. As the flow progresses through plane 7 and plane 8, the structure of the wake expands resulting in the distorted flow extending beyond the mean section towards the hub. The jet wake structure changes to a more uniform flow with pressure recovery, as the flow leaves the impeller and enters the vaneless diffuser. However, there is still low momentum fluid towards the tip section. A typical jet wake phenomenon is observed near the surge region on planes

7 and 8, with larger separated flow towards the tip section moving from mid passage towards the blade exit.

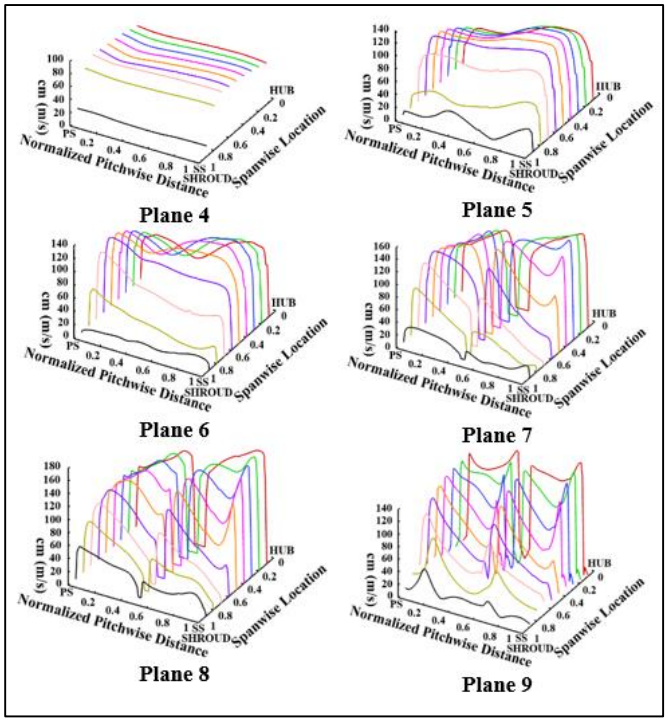

(a) without ported shroud

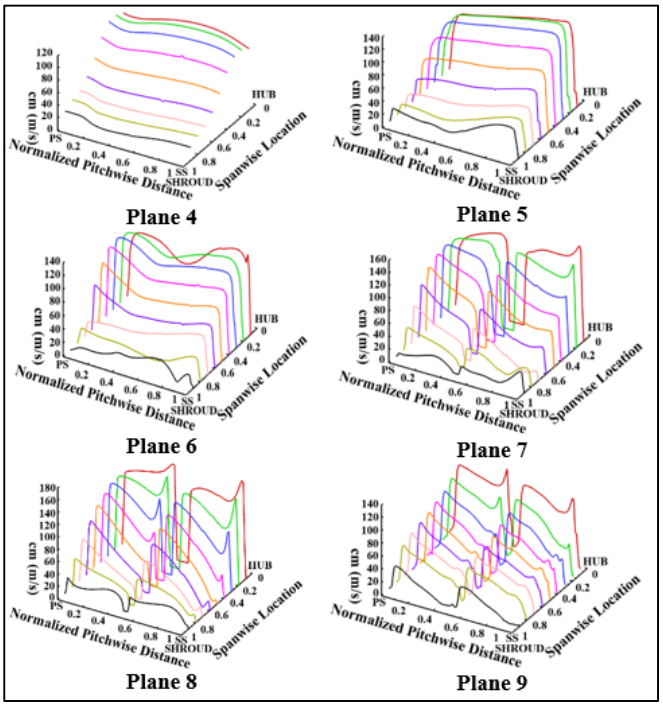

(b) with ported shroud

Figure 15: Meridional velocity distribution at different planes for case with ported shroud at near surge condition

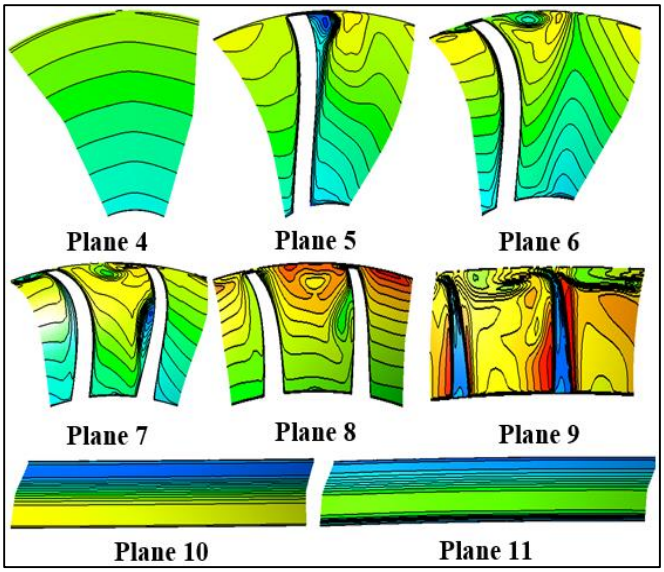

(a) without ported shroud

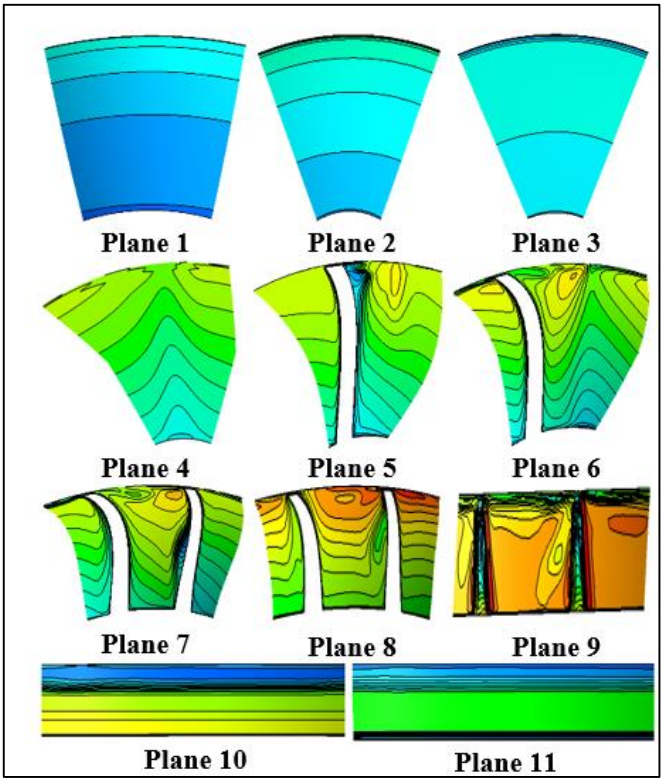

(b) with ported shroud

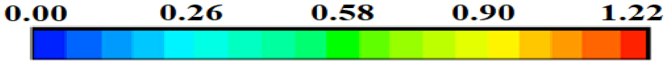

Figure 16: Relative Mach number contours near choke condition for configuration with ported shroud

From plane 4, (Figure 15b) it is observed that even though there is uniformity in the flow from hub to shroud, with introduction of ported shroud, there still exists region of

separated flow. Planes 5 and 6 have the higher velocity at hub section and the velocity reduces gradually from hub to shroud section with the ported shroud. The interaction of the leakage flow, the suction created by the ported shroud and vortices formed at the tip region result in slight reduction in flow velocity at shroud region.

This leads to a separated flow towards the impeller exit. Planes 7 and 8 have the jet wake at the suction side and on plane 9, at the impeller exit, jet wake has been reduced. However, since the low momentum fluid is sucked into the ported shroud, the flow at the exit gets more or less uniform. The uniformity of the flow at the exit and reduced jet wake at the exit could be the possible reasons for the increased operating range with better pressure recovery.

Figure 16 shows the contours of relative Mach number near choke condition, for the configuration without ported shroud (a) and with ported shroud (b). On plane 4, relative Mach number increases due to the suction created by the impeller and as the flow progresses, separation initiates at the shroud (Plane 5) resulting in the formation of a vortex near the tip section. Even though the flow splits into suction and pressure side flows, there is no significant region of low momentum fluid as the mass flow rate is higher during this condition. The pressure rise in the compressor during choke is significantly lower, due to which the pressure difference within the passage is also low.

In the case with ported shroud configuration (Figure 16b) near choke condition, the relative Mach number towards the tip region is higher as the flow progresses through the blade passage. This is because the additional fluid that is bypassed through the inducer is being injected into the main flow from the ported shroud. Further downstream of the impeller passage, the flow structure remains more or less similar in both cases, since the flow is almost choked for both configurations.

CONCLUSION

A turbocharger compressor has been designed from clean sheet in AxSTREAM® based on the given technical specifications in terms of operating pressure ratio and mass flow. A ported shroud has been introduced in the designed centrifugal compressor and the performance characteristics were obtained at design and off-design conditions for both baseline and ported shroud geometries. Performance comparison is done at three different speed lines. The observations that have been made from the above studies are as follows:

- Parametric studies were conducted to obtain the effect of ported shroud, at different axial locations along the blade axial length, on the operating range and performance of the turbocharger compressor. From these studies, the axial location 4.55 mm was found to be optimal.
- The location for the inlet of the ported shroud cavity should be ideally just downstream of the inducer and should not extend further into the impeller region.
- A comparison is done on the prediction of the meanline and 3D CFD solver. The variation in pressure ratio at design point between the two solvers is about 3% whereas for off-design conditions it extends to about 7%.
- By introducing the ported shroud, the operating range has been extended by 20.01% near surge and 5.18% near choke for the design speed with an efficiency increment near surge and a marginal decrement near choke.
- It is to be observed that as the axial distance of the ported shroud inlet (referenced from the impeller inlet) increases the difference in prediction between meanline solver and 3D CFD increases.
- The losses specified for the cavity tract in the meanline solver needs to change for different ported shroud location, however in the present case it was kept constant.
- Further studies needs to be done to evolve on the loss correlation for incorporating the same in meanline code.

REFERENCES

[1]. Fisher F. B. (1988), “Application of map width enhancement devices to turbocharger compressor stages” No.880794. SAE Technical Paper, 1988.

[2]. Chen, H., & Lei, V. M. (2013) “Casing treatment and inlet swirl of centrifugal compressors” Journal of Turbomachinery, Issue 135 volume 4.

[3]. Ramachandran, D., Mayandi, B., Krishnamoorthy, S., Mani, G., Ramesh, V., and Lakshmanan, S. C. (2017) “Development of Efficient Compressors for Turbochargers”, Proceedings of ASME TurboExpo 2017, June 26-30, 2017, Charlotte, NC, USA, GT2017-64359.

[4]. Sharma, S., Jupp, M. L., Nickson, A. K., and Allport, J. M. (2017), “Ported shroud flow processes and their effect on turbocharger compressor operation”, ASME TurboExpo 2017: Proceedings of ASME TurboExpo 2017, June 26-30, 2017, Charlotte, NC, USA, GT2017-63678.

[5]. Semlitsch, Bernhard, V. JyothishKumar, Mihai Mihaescu, Laszlo Fuchs, Ephraim Gutmark, and Matthieu Gancedo, (2014) “Numerical flow analysis of a centrifugal compressor with ported and without ported shroud” No. 2014-01-1655. SAE Technical Paper, 2014.

[6]. Guillou, E., Gancedo, M., and Gutmark, E. (2016). “Experimental investigation of flow instability in a turbocharger ported shroud compressor”, Journal of Turbomachinery, issue 138 volume 6.

[7]. Christou, G. A., Tan, C. S., Sirakov, B. T., Lei, V. M., and Alescio, G. (2017), “Characterizing Flow Effects of Ported Shroud Casing Treatment on Centrifugal Compressor Performance”, Journal of Turbomachinery, issue 139 volume 8.

[8]. AxSTREAM® user documentation 2017.

[9]. Leonid Moroz, Yuri Govorushenko, Petr Pagur, Leonid Romanenko, (2008) "Integrated Conceptual Design Environment for Centrifugal Compressor Flow Path Design" Proceedings of 2008 ASME International Mechancial Engineering Congress and Exposition, October 31 - November 6, 2008, Boston, Massachusetts, USA, IMECE 2008-69122.